ReScience

[Re] Cellular and Network Mechanisms of Slow Oscillatory Activity (<1 Hz) and Wave Propagations in a Cortical Network Model

Andrei Maksimov[1], **Sacha J. van Albada**[1], **and Markus Diesmann**[1,2,3]

1 Institute of Neuroscience and Medicine (INM-6) and Institute for Advanced Simulation (IAS-6) and JARA BRAIN Institute I, Jülich Research Centre, 52428 Jülich, Germany **2** Department of Psychiatry, Psychotherapy and Psychosomatics, Medical Faculty, RWTH Aachen University, 52062 Aachen, Germany **3** Department of Physics, Faculty 1, RWTH Aachen University, 52062 Aachen, Germany

maksimov.andrei7@gmail.com

Editor
Nicolas P. Rougier

Reviewers
Marcel Stimberg
Cyrille Rossant

Received June 28, 2016
Accepted October 11, 2016
Published October 17, 2016

Competing Interests:
The authors have declared that no competing interests exist.

A reference implementation of

→ *Cellular and network mechanisms of slow oscillatory activity (<1 Hz) and wave propagations in a cortical network model*, A. Compte, M.V. Sanchez-Vives, D.A. McCormick, X.-J. Wang, Journal of Neurophysiology, 2707–2725, 2003

Introduction

We provide an implementation of the model of [1], which reproduces single-neuron and collective network behaviors during slow-wave oscillations in vitro in control conditions and under pharmacological manipulations. In particular, we focus on the authors' model results that include: (a) neuronal membrane potentials oscillating between Up and Down states at <1 Hz; (b) characteristic membrane resistance behavior and activation of neuronal ion channels with proportional excitation and inhibition during Up states; (c) spontaneous and stimulus-evoked initiation and further wave-like propagation of population spiking activity. The original implementation is in C++, but the source code is not publicly available. The implementation we propose is coded in the NEST [5] framework, one of the modern actively developed simulation platforms that is publicly available. The code uses the Python interface [4] for legibility. The model and analysis scripts are implemented using Python 3.5.2, and also tested with Python 2.7.6.

Methods

We use the description of the model given in the original study, with the exception of the synaptic kinetics, which is greatly simplified (see model description below). In the original model, the majority of parameters are given per unit membrane surface area. For simplicity, we combine these parameters with the surface areas of the corresponding compartments in the following description. The resulting parameters are denoted with a tilde.

The model for excitatory neurons contains a somatic and a dendritic compartment. The somatic compartment includes fast Na^+ and K^+ spiking currents ($\widetilde{I}_{Na}$, $\widetilde{I}_{K}$), a

leak current $\widetilde{I}_{\mathrm{L}}$, a fast A-type K^+ current $\widetilde{I}_{\mathrm{A}}$, a non-inactivating slow K^+ current $\widetilde{I}_{\mathrm{KS}}$, and a Na^+-dependent K^+ current $\widetilde{I}_{\mathrm{KNa}}$. The dendritic compartment includes a high-threshold Ca^{2+} current $\widetilde{I}_{\mathrm{Ca}}$, a Ca^{2+}-dependent K^+ current $\widetilde{I}_{\mathrm{KCa}}$, a non-inactivating (persistent) Na^+ current $\widetilde{I}_{\mathrm{NaP}}$, and an inward rectifier (activated by hyperpolarization) non-inactivating K^+ current $\widetilde{I}_{\mathrm{AR}}$. Somato-dendritic coupling is implemented through the axial dendritic conductance g_{sd}. Non-synaptic currents are modeled using the Hodgkin-Huxley formalism $\widetilde{I}(t) = \tilde{g} m^k h^l (V - E_{\mathrm{rev}})$, where gating variables m and h are calculated using a first-order activation scheme, $\frac{dx}{dt} = \phi[\alpha(V)(1-x) - \beta(V)x] = (x_\infty(V) - x)/\tau(V)$ with $x_\infty = \frac{\alpha}{\alpha+\beta}$, $\tau = \frac{1}{\phi(\alpha+\beta)}$, and ϕ being the temperature factor (constant). In cases where time dependence is neglected (due to rapid activation or inactivation), gating variables are substituted by their saturation levels m_∞ or h_∞. The concentration of intrinsic neuronal Ca^{2+} and Na^+ ions (in mM) is drawn from first-order differential equations $\frac{d[\mathrm{Ca}^{2+}]}{dt} = \alpha_{\mathrm{Ca}}\widetilde{I}_{\mathrm{Ca}} - [\mathrm{Ca}^{2+}]/\tau_{\mathrm{Ca}}$ and $\frac{d[\mathrm{Na}^+]}{dt} = \alpha_{\mathrm{Na}}(\widetilde{I}_{\mathrm{Na}} + \widetilde{I}_{\mathrm{NaP}}) - R_{\mathrm{pump}}\left([\mathrm{Na}^+]^3 / \left([\mathrm{Na}^+]^3 + 15^3\right) - [\mathrm{Na}^+]^3_{\mathrm{eq}} / \left([\mathrm{Na}^+]^3_{\mathrm{eq}} + 15^3\right)\right)$ where α_{Ca}, α_{Na}, τ_{Ca}, R_{pump}, $[\mathrm{Na}^+]_{\mathrm{eq}}$ are constants. The model for inhibitory neurons just consists of a somatic compartment with only $\widetilde{I}_{\mathrm{Na}}$, $\widetilde{I}_{\mathrm{K}}$, and $\widetilde{I}_{\mathrm{L}}$ currents. AMPA and NMDA synaptic inputs target the dendritic compartment for excitatory and the somatic compartment for inhibitory neurons. GABA inputs always target the somatic compartment.

Because of the complexity of the single-neuron model (with multiple voltage-dependent channels), we verify that our implementation behaves like the original according to the information given in the paper. Similar to the original work, 500 ms injection of 250 pA current into the soma (Fig. 1) results in an adapting firing pattern in pyramidal (PY) and non-adapting firing in fast-spiking (FS) neurons with average firing rates of 22 and 76 spikes/s, respectively. Distribution of the membrane leak conductance with 10% (PY) and 2.5% (FS) standard deviation around the mean value leads to a small fraction of PY and a negligible fraction of FS neurons showing spontaneous activity.

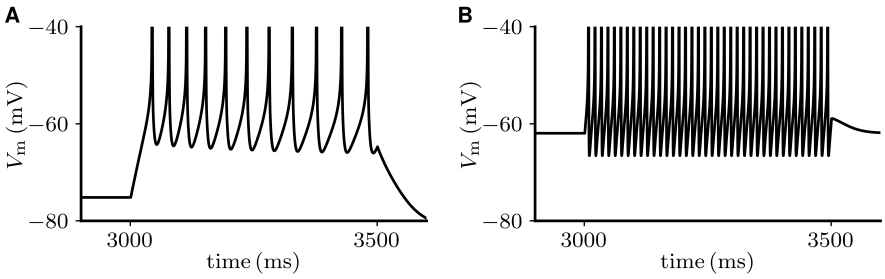

Figure 1: Model response to 250 pA current injection for 500 ms into the soma of a pyramidal (PY) (A) and a fast-spiking (FS) (B) neuron. The respective mean rates of 22 spikes/s for the PY neuron and 76 spikes/s for the FS neuron over the input period match those in the original implementation of Compte et al. [1].

The notable difference in our implementation is the synaptic kinetics. In the original model, synaptic gating variables depend on the presynaptic membrane potential. Implementing such a dependence is at present highly nontrivial in NEST due to optimizations for distributed computing (see Kunkel et al. [8], Hahne et al. [6] for background). For this reason, we simplify the synapse models while preserving the amplitude and shape of postsynaptic conductances. Specifically, the first-order kinetics of AMPA and GABA channels is replaced by a simple exponential decay $\frac{\partial g}{\partial t} = \sum_i W\delta(t - t_i) - \frac{g}{\tau}$, where g is the synaptic conductance, τ is the synaptic decay time, W is the synaptic weight, and i indexes the incoming spike times. The second-order kinetics of NMDA channels is substituted by a difference of slow and fast exponential

components, $g^{\mathrm{NMDA}} = g^{\mathrm{NMDA}}_{\mathrm{slow}} - g^{\mathrm{NMDA}}_{\mathrm{fast}}$ with $\frac{dg_{\mathrm{slow/fast}}}{dt} = \sum_i W\delta(t - t_i) - \frac{g_{\mathrm{slow/fast}}}{\tau_{\mathrm{slow/fast}}}$. These simplifications are justified by the stereotyped trajectory of the presynaptic membrane potential during an action potential. Further, these simplifications allow us to merge gating variables s of all synapses of one type (AMPA, NMDA or GABA) into a single postsynaptic time-dependent conductance (see Table 6). While multiple activations of the same synapse lead to linear summation of postsynaptic AMPA and GABA conductances in the original model, NMDA conductances saturate at high input rates. We model such behavior using the short-term plasticity formalism suggested by [11]. In short, the amplitude of the postsynaptic current $PSC = A \cdot R \cdot u$ is proportional to the fraction of available synaptic efficacy R and utilization of synaptic efficacy u. Spike-triggered synaptic activation leads to a reduction of the available synaptic efficacy (corresponding to short-term depression) together with an increase in the utilization of synaptic efficacy (corresponding to short-term facilitation). In the time period Δt between subsequent spikes, R and u recover to corresponding resting-state values ($R_0 = 1$ and $u_0 = U$) with time constants τ_{rec} and τ_{facil}. Our implementation closely follows the behavior of the original synapse model (Fig. 2). Note that the equation describing the dynamics of the NMDA gating variable s in the original paper contains a misprint and should read

$$\frac{ds}{dt} = \alpha(1 - s)x - s/\tau. \tag{1}$$

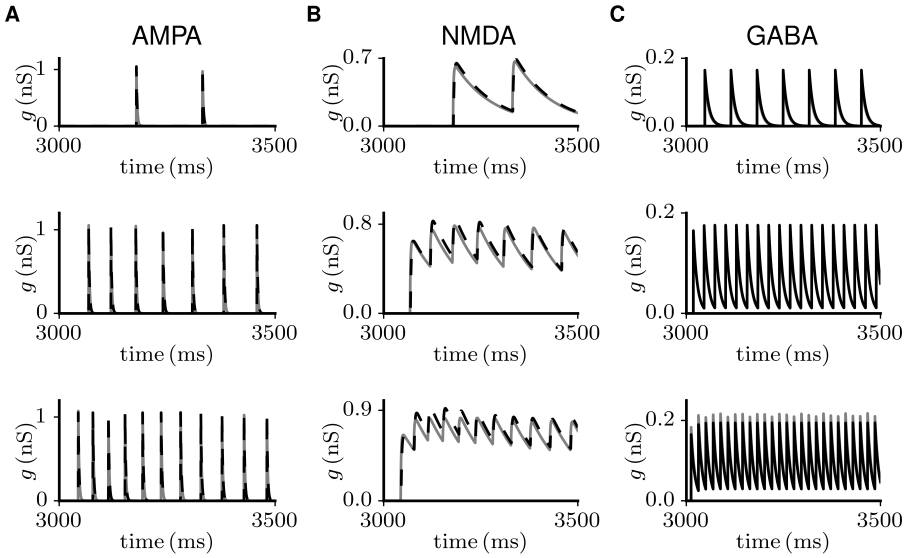

Figure 2: Simplified synaptic kinetics (dashed curve) for AMPA, NMDA, and GABA conductances closely reproduces the behavior of the original model (solid curve) in a wide range of spiking rates. DC currents, simultaneously injected into the soma of a presynaptic excitatory and an inhibitory neuron for 500 ms, lead to synaptic activation of the postsynaptic by the presynaptic neuron at rates of 4, 14, 22 spikes/s (top to bottom) for AMPA and NMDA, and 14, 36, 52 spikes/s for GABA channels. These synaptic activation rates span the range of excitatory and inhibitory neuronal firing rates observed during Up states in the model. Curves for the original model obtained with the help of a reimplementation of the single-neuron and synapse dynamics in Python. To construct this figure, synaptic inputs with a weight of $W = 1$ nS were provided to AMPA (A), NMDA (B), and GABA (C) channels for the original implementation. Note that due to gating variable s in the original implementation, the effective amplitude of a single synaptic input differs from the synaptic weight. For the implementation with simplified synaptic kinetics, synaptic weights are chosen to match the amplitude of the initial postsynaptic response in the original implementation.

The network architecture represents a chain of excitatory and inhibitory neurons

(of length l_{chain}) equidistantly distributed over 5 mm. Each neuron projects a given total number (drawn from a Gaussian distribution) of outgoing connections. The probability of a connection between any two neurons decays with inter-neuronal distance according to a Gaussian $P(x) = \exp(-\frac{x^2}{2\lambda^2})/\sqrt{2\pi\lambda^2}$ with characteristic scales λ_e and λ_i for excitatory and inhibitory presynaptic neuron types, respectively. Excitatory connections include both AMPA and NMDA channels, while inhibitory connections use GABA channels. Multiple connections can exist for a given pair of neurons. In Tables 1–7 we provide the description of the model.

The simulations are performed with NEST 2.8.0 [3] and combine an adaptive step size for the single-neuron solver with communication between neurons at a step size of 0.1 ms. The time resolution of all recordings is 0.1 ms.

In Fig. 6E excitatory and inhibitory conductances are filtered with a 40 ms rectangular kernel. This kernel width is chosen to yield average input levels, rather than individual synaptic events. We find that filtering is required to reproduce the proportionality of excitatory and inhibitory conductances, shown in the original Figure 6, although no corresponding information is given in the original paper.

To estimate the neuronal membrane conductance according to Eq. 3 in the model at a time t_0 near the membrane potential V_0, we use a procedure we refer to as the "virtual hyperpolarization method" (schematically shown in Fig. 3). First, an isolated copy of a neuron model instance is created with its state identical to that of the original neuron at the time of interest t_0. Then, the neuron is allowed to relax to its equilibrium state, while being clamped to the corresponding membrane potential V_0. In this steady-state configuration, the total cross-membrane current I_0 is calculated as the sum of all channel currents according to Eq. 4. Then the neuron is slightly hyperpolarized to potential V_1 and the corresponding steady-state current I_1 is calculated. The ratio $\Delta I/\Delta V$ then gives an estimate of the membrane conductance at time t_0. This approach can be applied to the case where the membrane is approximately isopotential across the whole neuron (true for the present model). In case of more complex non-isopotential multi-compartment neurons, the corresponding equilibrium currents I_0 and I_1 should be estimated through direct simulation. Note that during this procedure the state of the synaptic input should be fixed at the level of time t_0.

The relaxation time constant of certain ion concentrations (e.g., 80–350 ms for intracellular Ca^{2+} [10], [12]) can be much larger than the membrane time constant (on average <20 ms at rest, e.g., [9]) in cortical neurons. Therefore, the typical duration of DC pulse injection (∼80 ms [2], [13]) used in experiments with active networks is enough to overcome the transient phase of prominent capacitive currents, while certain ion concentrations might be not equilibrated. In the present model, however, the membrane relaxation time constant reaches hundreds of milliseconds (see relaxation phase in Fig. 8), which makes it difficult to separate these two effects. Therefore, in our application of the virtual hyperpolarization method to the model we consider limit cases of both instantaneous (frozen) and equilibrated ion concentrations.

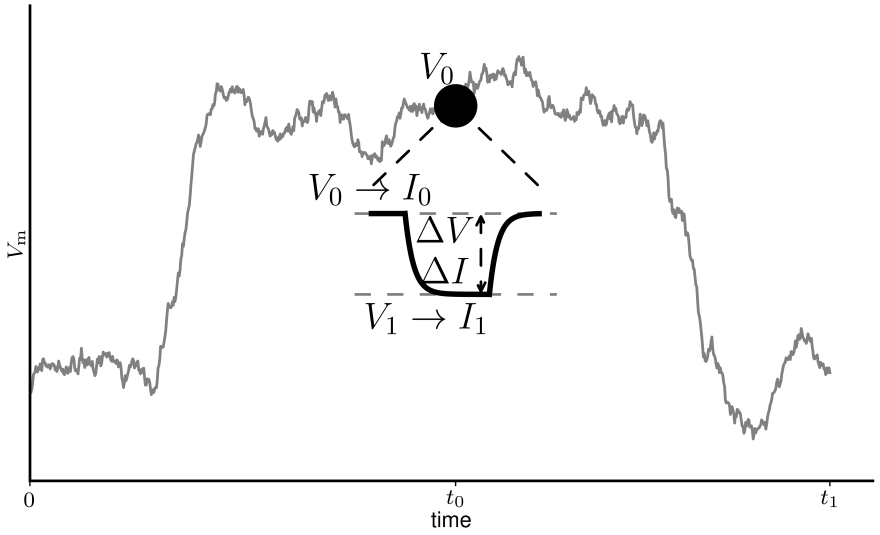

Figure 3: Schematic representation of the virtual hyperpolarization method. An isolated copy of a neuron model instance is created with its state identical to that of the original neuron at the time of interest t_0, including the level of synaptic input. Then the cross-membrane current I_0, required to keep the neuron clamped to membrane potential V_0 in the steady-state scenario, is determined. After that, the neuron is slightly hyperpolarized to the potential V_1 and the corresponding steady-state current I_1 is estimated. The resulting ratio $\Delta I/\Delta V$ then gives the conductance estimate at time t_0. In case of an isopotential neuron model, the corresponding currents I_0 and I_1 can be calculated using Eq. 4.

Table 1: Model summary.

Populations	one excitatory and one inhibitory cortical population
Topology	one-dimensional (chain); Gaussian spatial connectivity profile
Connectivity	random connections with outdegree drawn from a Gaussian distribution
Neuron model	single or multi-compartment Hodgkin-Huxley-type model with multiple channel types
Channel model	Hodgkin-Huxley formalism
Synapse model	single- or double-exponential-shaped postsynaptic conductances
Plasticity	presynaptic short-term plasticity
External input	None
Recordings	Spike times from all neurons; membrane potential, Na^+ and Ca^{2+} concentrations, and all conductances and currents from a subset of neurons in both populations

Table 2: Network topology and synapse model.

Connectivity paradigm		number (drawn from Gaussian distribution) of outgoing connections are randomly distributed across the target population with probability drawn from a Gaussian inter-somatic distance-dependent profile; multiple connections for the same pair of neurons are allowed; autapses are forbidden
Synaptic weights		same for all connections of the same type
Synaptic delays		same for all connections
Synaptic model		static synapse for connections to AMPA and GABA channels: $PSC_i = W$ synapse with short-term plasticity according to [11] for NMDA channels: $PSC_{i+1} = W \cdot R_{i+1} \cdot u_{i+1}$ $R_{i+1} = 1 + (R_i - R_i u_i - 1) \cdot \exp(-\delta t/\tau_{\text{rec}})$ $u_{i+1} = U + u_n (1 - U) \exp(-\delta t/\tau_{\text{fac}})$
N_e	1024	number of excitatory neurons
N_i	256	number of inhibitory neurons
λ_e	250	characteristic scale of spatial connectivity decay (μm) for excitatory connections
λ_i	125	characteristic scale of spatial connectivity decay (μm) for inhibitory connections
l_{chain}	5000	chain length (μm)
outdegree	20 ± 5	mean and standard deviation of Gaussian distribution used to determine numbers of outgoing connections for each neuron

Table 3: Neuron model and postsynaptic conductances. Ionic concentrations are measured in mM.

Neuron model	Hodgkin-Huxley-type model with multiple channel types and exponential-based synaptic conductances; two compartments for excitatory and one compartment for inhibitory neurons.
Subthreshold dynamics for PY neurons	soma: $C_\mathrm{m}\frac{dV}{dt} = -\left(\widetilde{I}_\mathrm{L} + \widetilde{I}_\mathrm{Na} + \widetilde{I}_\mathrm{K} + \widetilde{I}_\mathrm{A} + \widetilde{I}_\mathrm{KS} + \widetilde{I}_\mathrm{KNa} + g_\mathrm{sd}\left(V_\mathrm{d} - V_\mathrm{s}\right) + I_\mathrm{GABA}\right)$ dendrite: $C_\mathrm{m}\frac{dV}{dt} = -\left(\widetilde{I}_\mathrm{Ca} + \widetilde{I}_\mathrm{KCa} + \widetilde{I}_\mathrm{NaP} + \widetilde{I}_\mathrm{AR} + g_\mathrm{sd}\left(V_\mathrm{s} - V_\mathrm{d}\right) + I_\mathrm{AMPA} + I_\mathrm{NMDA}\right)$
Subthreshold dynamics for FS neurons	soma: $C_\mathrm{m}\frac{dV}{dt} = -\left(\widetilde{I}_\mathrm{L} + \widetilde{I}_\mathrm{Na} + \widetilde{I}_\mathrm{K} + I_\mathrm{AMPA} + I_\mathrm{NMDA} + I_\mathrm{GABA}\right)$
Spike detection	A spike is detected when the somatic membrane potential rises above 0 mV and its derivative becomes negative: $(V_s > 0) \wedge \left(\frac{dV_s}{dt} < 0\right)$. After that, the neuron becomes refractory and no spike emission is allowed during a fixed time of 1 ms.
Postsynaptic conductances	$g_\mathrm{AMPA,GABA}(t) = w\exp\left(-t/\tau\right)$ $g_\mathrm{NMDA}(t) = w\left(\exp\left(-t/\tau_\mathrm{slow}\right) - \exp\left(-t/\tau_\mathrm{fast}\right)\right)$
Channel dynamics	Hodgkin-Huxley formalism $\widetilde{I}(t) = \tilde{g}m^k h^l\left(V - E_\mathrm{rev}\right)$; m, h follow a first-order activation scheme, $\frac{dx}{dt} = \phi\left[\alpha(V)(1-x) - \beta(V)x\right] = \left(x_\infty(V) - x\right)/\tau(V)$ with $x_\infty = \frac{\alpha}{\alpha+\beta}$, $\tau = \frac{1}{\phi(\alpha+\beta)}$
Ca^{2+} concentration	$\frac{d\left[\mathrm{Ca}^{2+}\right]}{dt} = -\alpha_\mathrm{Ca}\widetilde{I}_\mathrm{Ca} - \left[\mathrm{Ca}^{2+}\right]/\tau_\mathrm{Ca}$
Na^{+} concentration	$\frac{d\left[\mathrm{Na}^{+}\right]}{dt} = -\alpha_\mathrm{Na}(\widetilde{I}_\mathrm{Na} + \widetilde{I}_\mathrm{NaP}) - R_\mathrm{pump}\left(\left[\mathrm{Na}^{+}\right]^3/\left(\left[\mathrm{Na}^{+}\right]^3 + 15^3\right) - \left[\mathrm{Na}^{+}\right]_\mathrm{eq}^3/\left(\left[\mathrm{Na}^{+}\right]_\mathrm{eq}^3 + 15^3\right)\right)$

Table 4: Channel dynamics for excitatory neurons. Membrane and reversal potentials are measured in mV, conductances in nS, ionic concentrations in mM, and time constants in ms.

Fast sodium current, soma	activation variable m:
$\widetilde{I}_{\mathrm{Na}} = \tilde{g}_{\mathrm{Na}} m^3 h \left(V - E_{\mathrm{Na}}\right)$	$\alpha = 0.1 \left(V + 33\right) / \left(1 - \exp\left(-\left(V + 33\right)/10\right)\right)$
	$\beta = 4 \exp(-(V + 53.7)/12)$
	inactivation variable h:
	$\alpha = 0.07 \exp\left(-\left(V + 50\right)/10\right)$
	$\beta = 1/\left(1 + \exp\left(-\left(V + 20\right)/10\right)\right)$
	$\tau = \frac{1}{4(a+b)}$
Fast potassium current, soma	inactivation variable k:
$\widetilde{I}_{\mathrm{K}} = \tilde{g}_{\mathrm{K}} k^4 \left(V - E_{\mathrm{K}}\right)$	$\alpha = 0.01 \cdot \left(V + 34\right) / \left(1 - \exp\left(-\left(V + 34\right)/10\right)\right)$
	$\beta = 0.125 \cdot \exp\left(-\left(V + 44\right)/25\right)$
	$\tau = \frac{1}{4(a+b)}$
Leakage current, soma	
$\widetilde{I}_{\mathrm{L}} = \tilde{g}_{\mathrm{L}} \left(V - E_{\mathrm{L}}\right)$	
Fast A-type K^+ current, soma	activation variable m:
$\widetilde{I}_{\mathrm{A}} = \tilde{g}_{\mathrm{A}} m^3 h \left(V - E_{\mathrm{K}}\right)$	$m_\infty = 1/\left(1 + \exp\left(-\left(V + 50\right)/20\right)\right)$
	inactivation variable h:
	$h_\infty = 1/\left(1 + \exp\left(\left(V + 80\right)/6\right)\right)$
	$\tau = 15$
Non-inactivating K^+ current, soma	activation variable m:
$\widetilde{I}_{\mathrm{KS}} = \tilde{g}_{\mathrm{KS}} m \left(V - E_{\mathrm{K}}\right)$	$m_\infty = 1/\left(1 + \exp\left(-\left(V + 34\right)/6.5\right)\right)$
	$\tau = 8/\left(\exp\left(-\left(V + 55\right)/30\right) + \exp\left(\left(V + 55\right)/30\right)\right)$
Persistent Na^+ current, dendrite	activation variable m:
$\widetilde{I}_{\mathrm{Na}} = \tilde{g}_{\mathrm{NaP}} m^3 \left(V - E_{\mathrm{Na}}\right)$	$m_\infty = 1/\left(1 + \exp\left(-\left(V + 55.7\right)/7.7\right)\right)$
Inwardly rectifying K^+ current, dendrite	activation variable m:
$\widetilde{I}_{\mathrm{AR}} = \tilde{g}_{\mathrm{AR}} m \left(V - E_{\mathrm{K}}\right)$	$m_\infty = 1/\left(1 + \exp\left(\left(V + 75\right)\right)/4\right)$
High-threshold Ca^{2+} current, dendrite	activation variable m:
$\widetilde{I}_{\mathrm{Ca}} = \tilde{g}_{\mathrm{Ca}} m^2 \left(V - E_{\mathrm{Ca}}\right)$	$m_\infty = 1/\left(1 + \exp\left(-\left(V + 20\right)/9\right)\right)$
Na^+-dependent K^+ current, soma	activation variable m:
$\widetilde{I}_{\mathrm{KNa}} = \tilde{g}_{\mathrm{KNa}} m \left(V - E_{\mathrm{K}}\right)$	$m_\infty = 0.37/\left(1 + \left(38.7/\left[\mathrm{Na}^+\right]\right)^{3.5}\right)$
Ca^{2+}-dependent K^+ current, dendrite	activation variable m:
$\widetilde{I}_{\mathrm{KCa}} = \tilde{g}_{\mathrm{KCa}} m \left(V - E_{\mathrm{K}}\right)$	$m_\infty = \left[\mathrm{Ca}^{2+}\right] / \left(\left[\mathrm{Ca}^{2+}\right] + 30\right)$

Table 5: Channel dynamics for inhibitory neurons. Membrane and reversal potentials are measured in mV, conductances in nS, ionic concentrations in mM, and time constants in ms.

Fast sodium current, soma	activation variable m:
$\widetilde{I}_{\mathrm{Na}} = \tilde{g}_{\mathrm{Na}} m^3 h \left(V - E_{\mathrm{Na}}\right)$	$\alpha = 0.5\left(V+35\right) / \left(1 - \exp\left(-\left(V+35\right)/10\right)\right)$
	$\beta = 20 \exp\left(-\left(V+60\right)/18\right)$
	inactivation variable h:
	$\alpha = 0.35 \exp\left(-\left(V+58\right)/20\right)$
	$\beta = 5 / \left(1 + \exp\left(-\left(V+28\right)/10\right)\right)$
	$\tau = \frac{1}{(a+b)}$
Fast potassium current, soma	inactivation variable k:
$\widetilde{I}_{\mathrm{K}} = \tilde{g}_{\mathrm{K}} k^4 \left(V - E_{\mathrm{K}}\right)$	$\alpha = 0.05\left(V+34\right) / \left(1 - \exp\left(-\left(V+34\right)/10\right)\right)$
	$\beta = 0.625 \exp\left(-\left(V+44\right)/80\right)$
	$\tau = \frac{1}{(a+b)}$
Leakage current, soma	
$\widetilde{I}_{\mathrm{L}} = \tilde{g}_{\mathrm{L}} \left(V - E_{\mathrm{L}}\right)$	

Table 6: Parameter specification for our synaptic implementation. Note that the synaptic conductances differ with respect to the original implementation.

delay	0.1	synaptic delay (ms)
$W_{e \leftarrow \mathrm{AMPA}}$	7	synaptic weights (nS)
$W_{i \leftarrow \mathrm{AMPA}}$	3	
$W_{e \leftarrow \mathrm{NMDA}}$	0.15	
$W_{i \leftarrow \mathrm{NMDA}}$	0	
$W_{e \leftarrow \mathrm{GABA}}$	16	
$W_{i \leftarrow \mathrm{GABA}}$	2	
U	0.5	initial utilization of synaptic efficacy
τ_{rec}	130	recovery time constant (ms) of available synaptic efficacy for NMDA synapses onto PY and FS neurons
τ_{facil}	0	recovery time constant (ms) of utilization of synaptic efficacy
τ_{AMPA}	2	time constant of AMPA channels (ms)
τ_{GABA}	10	time constant of GABA channels (ms)
$\tau^{\mathrm{slow}}_{\mathrm{NMDA}}$	100	slow time constant of NMDA channels (ms)
$\tau^{\mathrm{fast}}_{\mathrm{NMDA}}$	2	fast time constant of NMDA channels (ms)

Table 7: Parameter specification for our neuronal implementation. The superscripts soma and dendr refer to the somatic and dendritic compartments. When parameters for excitatory and inhibitory neurons are different, parameters for the latter are given in brackets. "(-)" means parameter not used for the inhibitory neuron model.

E_{Ca}	120	reversal potential of Ca^{2+} channels (mV)
E_{Na}	55	reversal potential of Na^{+} channels (mV)
E_{K}	$-100(-90)$	reversal potential of K^{+} channels (mV)
E_{L}	-60.95 ± 0.3 (-63.8 ± 0.15)	leak reversal potential (mV), mean and standard deviation of Gaussian distribution
E_{ex}	0	reversal potential AMPA and NMDA channels (mV)
E_{in}	-70	reversal potential GABA channels (mV)
$\tilde{C}_{m}^{soma}$	150(200)	somatic membrane capacitance (pF)
$\tilde{C}_{m}^{dendr}$	350(-)	dendritic membrane capacitance (pF)
$\tilde{g}_{Na}^{soma}$	7500 (7000)	maximal conductance of fast Na^{+} channel (nS)
$\tilde{g}_{K}^{soma}$	1575 (1800)	maximal conductance of fast K^{+} channel (nS)
$\tilde{g}_{L}^{soma}$	10 ± 1 (20.5 ± 0.5)	leak conductance (nS)
$\tilde{g}_{KA}^{soma}$	150 (-)	maximal conductance of A-type fast K^{+} channel (nS)
$\tilde{g}_{KNa}^{soma}$	200 (-)	maximal conductance of Na^{+}-dependent K^{+} channel (nS)
$\tilde{g}_{KS}^{soma}$	86.4 (-)	maximal conductance of non-inactivating K^{+} channel (nS)
$\tilde{g}_{KCa}^{dendr}$	200 (-)	maximal conductance of Ca^{2+}-dependent K^{+} channel (nS)
$\tilde{g}_{KAR}^{dendr}$	9 (-)	maximal conductance of inwardly rectifying K^{+} channel (nS)
$\tilde{g}_{NaP}^{dendr}$	24 (-)	maximal conductance of persistent Na^{+} channel (nS)
$\tilde{g}_{Ca}^{dendr}$	150.5 (-)	maximal conductance of high-threshold Ca^{2+} channel (nS)
g_{ax}	1750 (-)	axial dendritic conductance between somatic and dendritic compartments

Results

We here focus on the main activity regime of the model, namely Up-Down oscillations that are either spontaneously generated or induced by stimulation. First, we simulate the reimplemented model with the parameters corresponding to the original paper. The simulated activity, however, is characterized by unreasonably high firing rates due to the dominance of NMDA conductances far exceeding the potency of the opposing GABAergic inhibition. This difference from the original results might be a consequence of the different implementation of synaptic dynamics. Closer examination of the original Figure 5C suggests that unitary excitatory and inhibitory postsynaptic responses are approximately 0.5 nS during periods of network silence. This contradicts our implementation of the non-modified synaptic dynamics (see Fig. 2), where single synaptic activations (with synaptic weights as in the original model) would result in 5.4 and 0.8 nS postsynaptic response for AMPA and GABA channels, respectively. This suggests an inconsistency between the reported dynamics and that which was implemented already in the original work. Furthermore, we assumed the units of the function defining the dependence of the synaptic conductances on the presynaptic

membrane potential to be ms^{-1}, but this is not strictly specified in the original work, providing another potential source of discrepancies.

To achieve an appropriate network regime, we modify the synaptic strengths W of all synapse types. Specifically, we match the firing rates, the duration of Up and Down states, the wave propagation speed, and the response to network stimulation. Corresponding synaptic strengths for the model with simplified synaptic dynamics are given in Table 6. When transformed back to the original implementation (i.e., excluding the synaptic gating variable s), the modified strengths are $g_{\mathrm{ee}}^{\mathrm{AMPA}} = 6.6\,\mathrm{nS}$, $g_{\mathrm{ee}}^{\mathrm{NMDA}} = 0.1\,\mathrm{nS}$, $g_{\mathrm{ei}}^{\mathrm{AMPA}} = 2.8\,\mathrm{nS}$, $g_{\mathrm{ei}}^{\mathrm{NMDA}} = 0\,\mathrm{nS}$, $g_{\mathrm{ie}}^{\mathrm{GABA}} = 97\,\mathrm{nS}$, $g_{\mathrm{ii}}^{\mathrm{GABA}} = 12\,\mathrm{nS}$. However, a range of different synaptic weight settings was able to produce qualitatively identical network activity. Therefore, we chose a set of weights from among these possibilities based on relative proximity to the originally reported weight values. Besides the reasons mentioned above, differences between the simplified and original synaptic kinetics during network activity, not brought out by the simple inputs in Fig. 2, may contribute to the need for weight changes to obtain a network state similar to that in the original study. However, this is unlikely to account for the need to strongly increase the inhibitory weights relative to the excitatory ones. In the absence of the original code and since our network implementation does not allow using the original synapse dynamics, we cannot resolve this issue here.

The adjusted weights result in periods of spontaneously generated activity (Up states) which propagate along the network in a wave-like fashion (Fig. 4A) with propagation speed $3 - 7\,\mathrm{mm/s}$. On the level of individual neurons, Up states are characterized by a depolarized membrane potential and an increase of the intracellular concentration of Na^+ ions by 3–4.5 mM (Fig. 4C,D for two neurons), similar to the results shown in Figure 2 of the original work. When excitatory neurons are slightly hyperpolarized to reduce the level of spontaneous activity, external stimulation of 40 adjacent excitatory neurons can initiate Up state propagation (Fig. 5A) with the firing rate profiles (Fig. 5C) being similar to those shown in Figure 3D of the original work. The histogram of the intervals between the first spike of each pyramidal cell and its immediately adjacent interneuron (Fig. 5B) closely resembles the original result in Figure 3C. In analogy to the original work, repeated network stimulation within a few seconds after the first one does not evoke an Up state transition (Fig. 5A).

During the spontaneous Up-Down oscillations shown in Fig. 4A, synaptic and intrinsic neuronal conductances (Fig. 6B–I) are tightly coupled to the membrane depolarization (Fig. 6A) and show a dynamic range very similar to that reported in the original Figure 5. When filtered with a rectangular kernel (see Methods), excitatory and inhibitory conductances are clearly coupled (Fig. 6E), like in the original model (see their Figure 6).

When computed as the reciprocal of the sum of all conductances (see Eq. 2), membrane resistance is decreased during Up states relative to silent Down states (Fig. 6B, 7), consistent with the results shown in Figure 5B of the original work. We also estimated membrane resistance by injecting hyperpolarizing DC pulses (300 pA for 100 ms) into neurons, constantly hyperpolarized by 250 pA current injection (see Fig. 7A), similar to the way described in the original Figure 4. In agreement with the original paper, the resulting membrane resistance, computed as the voltage deflection at the end of the pulse divided by the pulse amplitude (Fig. 7B dots) is quantitatively similar to the values obtained with the reciprocal of Eq. 2 (Fig. 7 solid line) at least for membrane potentials below $-80\,\mathrm{mV}$.

However, note that the authors define membrane conductance as

$$G_{\mathrm{m}}^{\mathrm{model}} = \sum_i G_i\,(V) \tag{2}$$

where G_i are the instantaneous conductances of all ionic channels, which are typically time- and voltage-dependent. This definition corresponds to the "instantaneous chord conductance" according to the classification given by [7]. In contrast, the typical

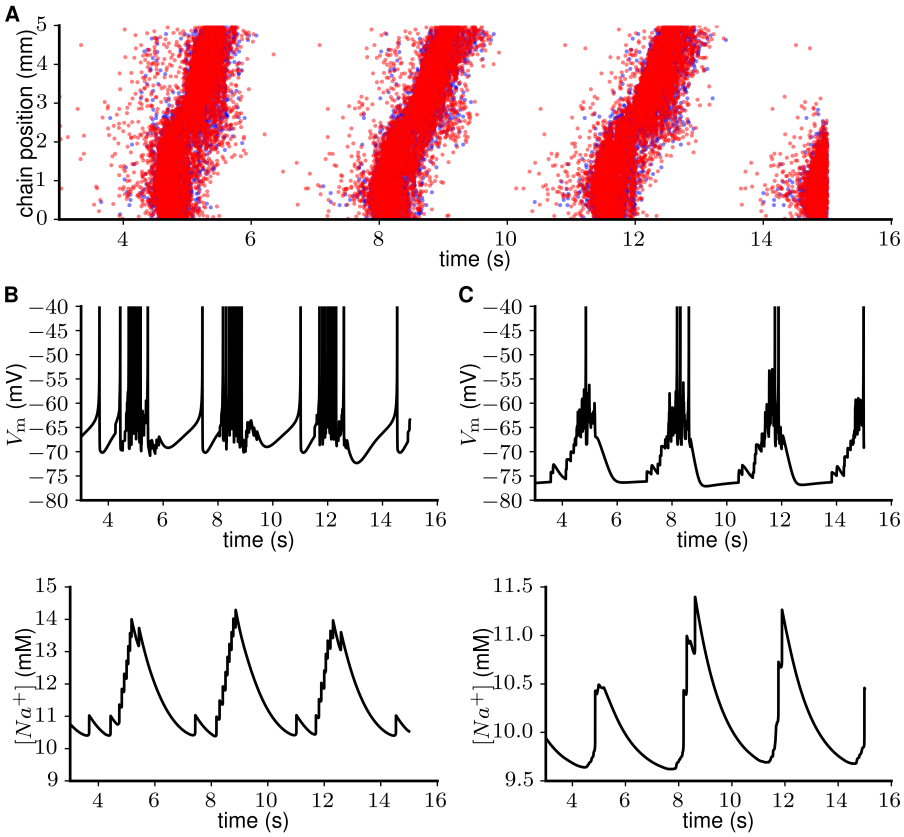

Figure 4: Spontaneous Up-Down oscillations generated in a network of 1280 neurons with a chain-like architecture. (A) Spiking activity of excitatory (red) and inhibitory (blue) neurons propagates along the chain in a wave-like fashion. **(B, C)** Intracellularly recorded membrane potentials (top) and concentration of intracellular Na^+ ions (bottom) of PY neurons are similar to those reported in the original study (their Figure 2). The neuron in **B** shows spontaneous activity with spiking during Down states, while the neuron in **C** is typical for the majority of neurons and is characterized by well-defined Up and Down states.

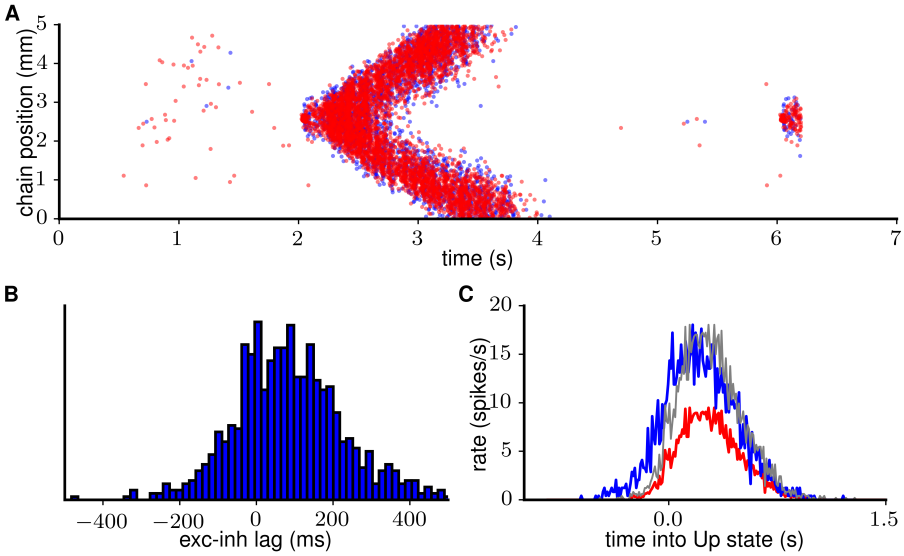

Figure 5: Transition to Up state is evoked by external stimulation in a network of 1280 neurons with a chain-like architecture. (A) Spiking activity of excitatory (red) and inhibitory (blue) neurons propagates along the chain in a wave-like fashion when stimulated at time $t = 2\,\mathrm{s}$. Stimulation at $t = 6\,\mathrm{s}$, however, does not evoke a transition to the Up state. All excitatory neurons are continuously hyperpolarized by $5\,\mathrm{pA}$ external current to reduce spontaneous activity. Network stimulation is achieved by injection of $200\,\mathrm{pA}$ current for $50\,\mathrm{ms}$ into 40 adjacent excitatory neurons. **(B)** Histogram of the intervals between the first spike of each pyramidal cell and its immediately adjacent interneuron in the time window shown in **A**. **(C)** Firing rate averaged across neurons for the time window shown in **A**. We substract from the spike times for each excitatory (inhibitory) neuron the time of the first spike of the nearest inhibitory (excitatory) neuron, and then we construct the time histogram of those intervals in the red (blue) curve. Gray curve represents the red curve scaled to match the peak value of the blue curve.

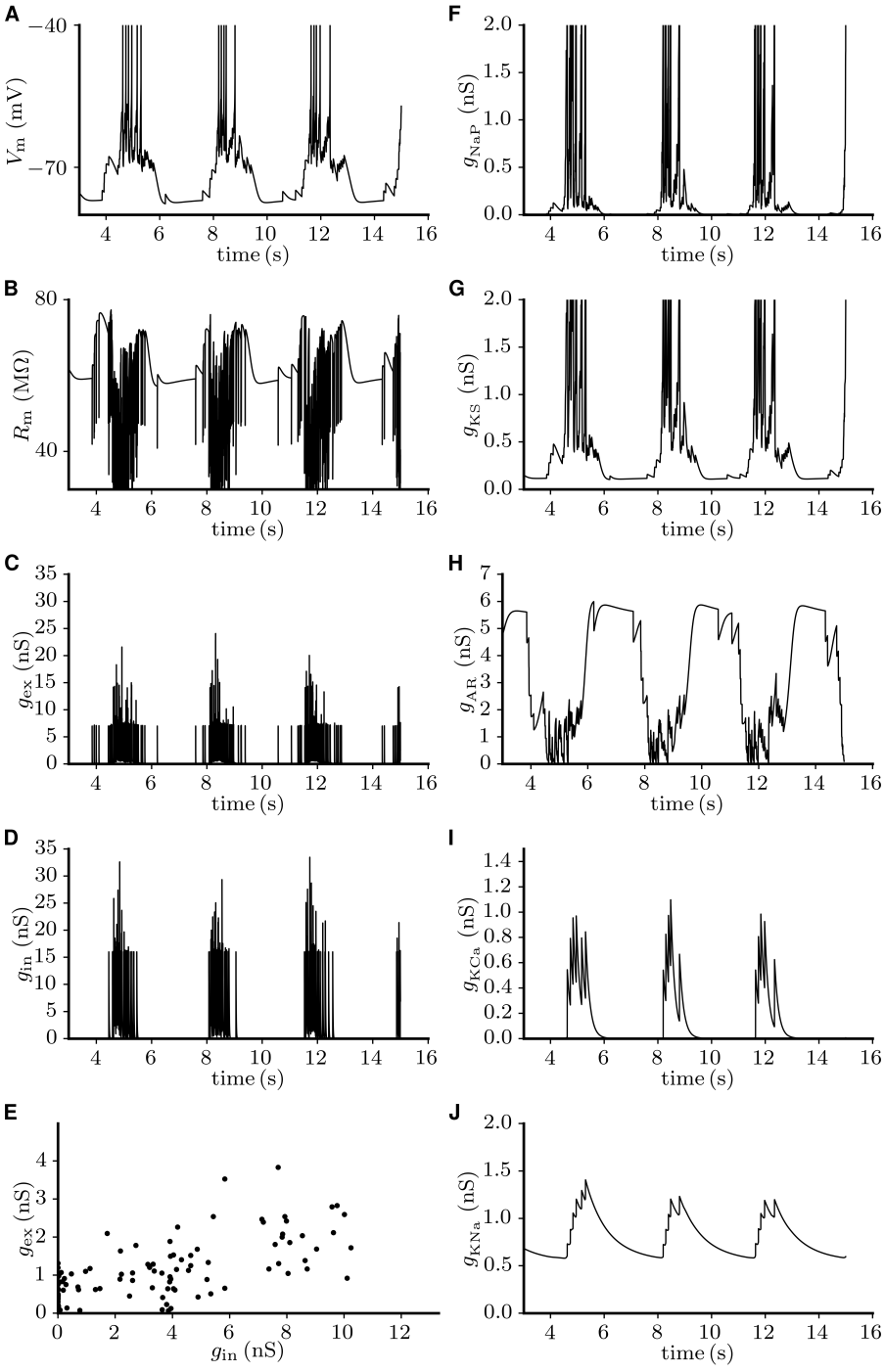

Figure 6: Membrane input resistance and various ionic conductances in the course of the slow oscillation on the example of a representative neuron. (A) Membrane voltage trace shows periods of high activity (Up states). **(B)** Total input resistance, measured as the reciprocal of the summed open membrane conductances. Excitatory and inhibitory synaptic conductances **(C, D)** are approximately proportional when binned with $40\,\mathrm{ms}$ bin width **(E)**. **(F-J)** The dynamics of various other conductances ($\tilde{g}_{\mathrm{NaP}}$; $\tilde{g}_{\mathrm{KS}}$; $\tilde{g}_{\mathrm{KAR}}$; $\tilde{g}_{\mathrm{KCa}}$; $\tilde{g}_{\mathrm{KNa}}$) closely resembles that reported in the original paper (their Figure 5).

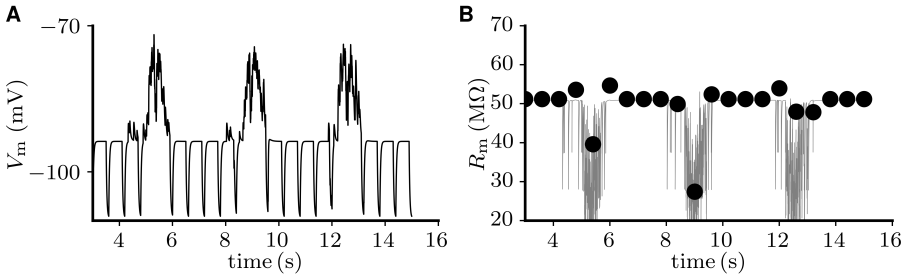

Figure 7: Accessing neuronal membrane resistance through the reciprocal of the sum of open channel conductances and through the injection of brief hyperpolarizing pulses results in quantitatively similar estimates. (A) Membrane voltage trace in response to 100 ms hyperpolarizing pulses with amplitude 300 pA while the neuron is continuously hyperpolarized by a 250 pA current, similarly to the procedure described in the original Figure 4. **(B)** Gray trace, resistance corresponding to the trace in **A** as determined by the reciprocal of the sum of open channel conductances. Black dots, corresponding resistance as estimated from the injection of hyperpolarizing pulses.

experimentally measured quantity corresponds to "steady-state slope conductance" from the same classification:

$$G_{\mathrm{m}}^{\mathrm{exp}} = \frac{\Delta I}{\Delta V} \tag{3}$$

where ΔI is the extra current (injected into the soma) required to achieve a steady-state membrane potential shift $\Delta V = V - V_0$ from the initial level V_0 (prior to current injection). The steady state here refers to the situation where transient capacitive currents become negligible. To compare these two definitions we use the fact that in the steady-state case, the externally injected current I is equal to minus the sum of all ionic currents,

$$I = \sum_i G_i\left(V\right) \cdot \left(V - E_i\right), \tag{4}$$

where E_i is the reversal potential of channel i. Combining Eqs 3 and 4 and using

$$\begin{aligned}\Delta\left(G_i\left(V\right) \cdot \left(V - E_i\right)\right) &= \Delta\left(G_i\left(V\right)\right) \cdot \left(V - E_i\right) + G_i\left(V\right) \cdot \Delta\left(V - E_i\right) \\ &= \Delta\left(G_i\left(V\right)\right) \cdot \left(V - E_i\right) + G_i\left(V\right) \cdot \Delta V\end{aligned}$$

results in an overall membrane conductance

$$G_{\mathrm{m}}^{\mathrm{exp}} = \sum_i \frac{\Delta\left(G_i\left(V\right) \cdot \left(V - E_i\right)\right)}{\Delta V} = \sum_i \frac{\Delta\left(G_i\left(V\right)\right)}{\Delta V}\left(V - E_i\right) + \sum_i G_i\left(V\right). \tag{5}$$

As one can see, the definition used in the original study (Eq. 2) excludes the first term. To demonstrate the difference in these two definitions, we simulate isolated pyramidal neurons (parameters are set to average values) with DC inputs of different amplitudes injected for 20 seconds into the soma and record the membrane potential (Fig. 8A) as well as all ionic channel conductances. A long pulse duration is chosen here to take into account the long time required for the model neuron to reach a steady state. Then we compute membrane conductance according to Eq. 5 and Eq. 2 a few milliseconds before the DC input is switched off. The I-V curve shows a profound nonlinearity (Fig. 8B) leading to $G_{\mathrm{m}}^{\mathrm{exp}}$ (the reciprocal of the slope of the I-V curve) reaching 0.012 nS (corresponding to 83 GΩ), while $G_{\mathrm{m}}^{\mathrm{model}}$ remains near 15 nS (corresponding to 0.07 GΩ) (Fig. 8C). Therefore, under the protocol mimicking a standard electrophysiological procedure, the instantaneous chord and steady-state slope conductances deviate by

several orders of magnitude for the present neuron model. To measure the steady-state slope conductance (Eq. 3) during ongoing network activity in the model, we use the virtual hyperpolarization method (see Methods). Freezing the state of the neuron as done in this method is necessary because of the aforementioned long relaxation time of the model neurons, which necessitates pulse durations that exceed the length of an Up state and therefore prevents measuring steady-state resistances during freely evolving activity. The results of this method for the above case of prolonged DC stimulation closely match those obtained from the I-V curve (Fig. 8C). In the active network model, this method results in a membrane conductance around 2 nS (corresponding to 500 MΩ) during the Down state (Fig. 9B,C). During the Up states, however, membrane conductance tends to drop to zero and even becomes negative for $5 - 75$ ms with an average of 32 ms before oncoming spike events, indicating self-depolarizing dynamics in the subthreshold periods. Note that in Fig. 9B,C time periods of 5 ms before and after each spike event are not considered to avoid the contamination of subthreshold dynamics with spikes.

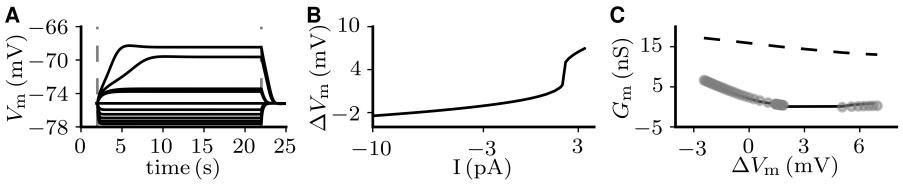

Figure 8: The method of accessing neuronal membrane conductance (or resistance) suggested by [1] deviates from the approach based on the construction of an I-V curve. (A) A 10 s DC injection (inside the region marked by vertical dashed lines) with various amplitudes into the somatic compartment of a PY neuron results in neuronal hyper-/depolarization. Relaxation of membrane potentials after offset of the DC input takes hundreds of ms. **(B)** The I-V curve shows a strong voltage dependence of the neuronal resistance (measured as the slope of the curve). **(C)** Membrane conductance measured with the method suggested by the authors of [1] (Eq. 2; dashed curve), is around 15 nS (corresponding to a 70 MΩ resistance) for the neuron being hyper- or depolarized by $\Delta V = -3$–7 mV by DC currents. Membrane conductance measured according to Eq. 5 (solid curve), reaches 0.012 nS (corresponding to a 83 GΩ resistance). The virtual hyperpolarization method (circles, see Methods) closely reproduces the latter conductance measure.

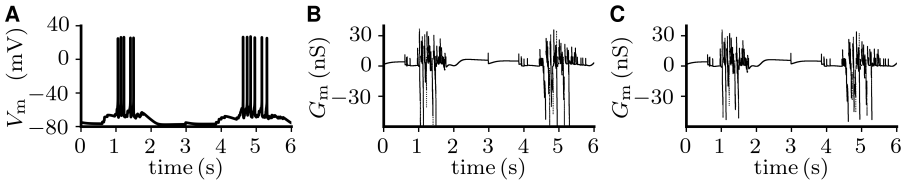

Figure 9: Application of the virtual hyperpolarization method to the network model. Neuronal depolarization during Up states **(A)** is associated with dominant strongly negative membrane conductance **(B,C)**, which is the result of self-depolarization due to intrinsic neuronal dynamics. Membrane conductance is calculated according to Eq. 3 with Na^+ and Ca^{2+} frozen **(B)** and steady-state **(C)**. The time windows of 5 ms just before and after individual spikes are masked in the determination of the conductance to avoid contamination by supra-threshold activity.

Finally, in the original work modification of e-to-i and i-to-e synaptic weights by 10% results in noticeable differences in spiking activity, though oscillations are qualitatively preserved (see their Figure 6). In our model, however, similar modification of synaptic weights results in negligible differences in spiking activity. Also, when AMPA, NDMA, or GABA conductances are blocked in the model, corresponding changes in the spiking pattern are similar in the original (their Figure 9) and the present model

(Fig. 10).

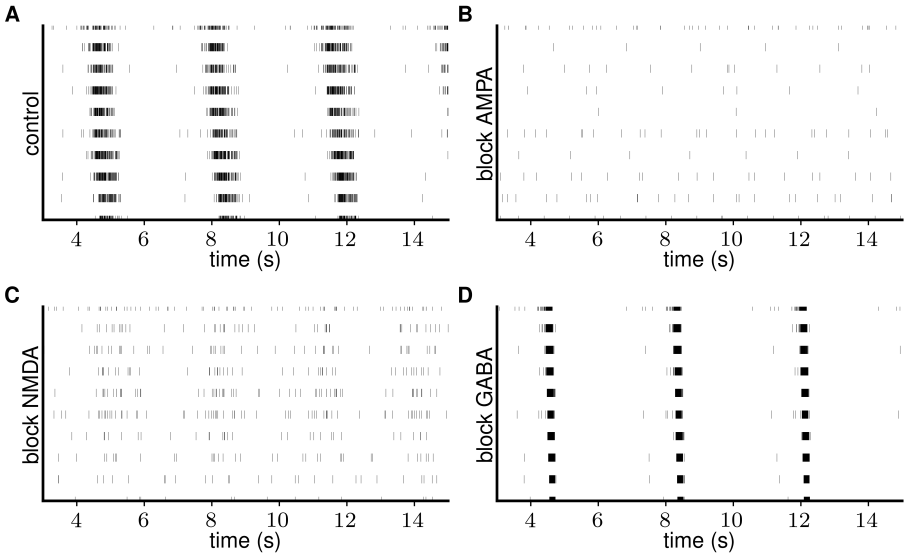

Figure 10: When AMPA, NMDA, or GABA channels are blocked in the model, simulation reproduces the results reported in the original Figure 9. Spiking activity is visualized as multi-unit recordings with recording sites spatially separated by $250\,\mu$m. Each site records from neurons within a $50\,\mu$m range.

Conclusion

After modifications to the model with respect to synaptic dynamics and strength, we are able to reproduce the majority of the original results concerning spontaneously generated and stimulation-evoked Up-Down oscillations. In particular, the dynamics of membrane potentials, membrane resistances, channel conductances, intracellular concentrations of Na^+ and Ca^{2+} ions, and spiking activity closely resemble those of the original model. In our implementation, the synaptic dynamics does not depend on the shapes of individual presynaptic action potentials, but just incorporates the average postsynaptic effect of an action potential. The fact that we can reproduce the emerging network phenomena suggests that this detail of the synapse model is not relevant on the network level. We provide a closer look at the method which the authors of the original study use to access neuronal conductance (or resistance). Their measure reflects an "instantaneous chord conductance", which results in the model in values around 15 nS in an isolated pyramidal neuron, and around 20 nS throughout network activity. In experimental works, the typical measure approximates a "steady-state slope conductance" (see [7] for classification), which results in a membrane conductance of less than 1 nS for a slightly depolarized isolated pyramidal neuron. Throughout network activity, this yields around 2 nS during Down states, strongly fluctuating membrane conductance during subthreshold Up state periods, and a strong negative conductance lasting on average 32 ms before each spike event. These low and even negative long-lasting conductances are typically not reported in the experimental literature. Therefore, the dynamics of membrane conductance in the model merits further investigation. The present model successfully reproduces the network response to blockade of AMPA, NMDA, or GABA channels. However, the sensitivity of the present model to changes in the synaptic strengths is weaker than in the original model.

We could not obtain the desired network regime with the synaptic weights reported

in the original work after calibration to account for the change in the synaptic model. We suggest the synaptic dynamics to be the source of discrepancy, as suggested by the inconsistency between our synapse implementation and the results shown in the original Figure 5C.

Apart from these differences in synaptic dynamics, we confirm the correctness of the original implementation of the model.

Acknowledgements

Partly supported by by Helmholtz Portfolio Supercomputing and Modeling for the Human Brain (SMHB), EU Grant 269921 (BrainScaleS), and EU Grant 604102 (Human Brain Project, HBP). All network simulations carried out with NEST (http://www.nest-simulator.org).

References

[1] A. Compte et al. "Cellular and network mechanisms of slow oscillatory activity (<1 Hz) and wave propagations in a cortical network model". In: *J. Neurophysiol.* 89 (2003), pp. 2707–2725.

[2] D. Contreras, I. Timofeev, and M. Steriade. "Mechanisms of long-lasting hyperpolarizations underlying slow sleep oscillations in cat corticothalamic networks". In: *J. Physiol. (Lond)* 494.1 (1996), pp. 251–264.

[3] J.M. Eppler et al. *NEST 2.8.0*. 2015. URL: http://dx.doi.org/10.5281/zenodo.32969.

[4] J.M. Eppler et al. "PyNEST: a convenient interface to the NEST simulator". In: *Front. Neuroinformatics* 2 (2009), p. 12.

[5] M. Gewaltig and M. Diesmann. "NEST (NEural Simulation Tool)". In: *Scholarpedia* 2.4 (2007), p. 1430.

[6] J. Hahne et al. "A unified framework for spiking and gap-junction interactions in distributed neuronal network simulations." In: *Front. Neuroinform.* 9.22 (2015).

[7] J.J.B. Jack, D. Noble, and R.W. Tsien. *"Electric Current Flow in Excitable Cells"*. Oxford: Oxford University Press, 1983.

[8] S. Kunkel et al. "Spiking network simulation code for petascale computers". In: *Front. Neuroinform.* 8 (2014), p. 78.

[9] R.B. Levy and A.D. Reyes. "Spatial profile of excitatory and inhibitory synaptic connectivity in mouse primary auditory cortex." In: *J. Neurosci.* 32.16 (2012), pp. 5609–5619.

[10] H. Markram, P.J. Helm, and B. Sakmann. "Dendritic calcium transients evoked by single back-propagating action potentials in rat neocortical pyramidal neurons." In: *J Physiol.* 485 (1995), pp. 1–20.

[11] H. Markram, Y. Wang, and M. Tsodyks. "Differential signaling via the same axon of neocortical pyramidal neurons". In: *PNAS* 95.9 (1998), pp. 5323–5328.

[12] J. Schiller, F. Helmchen, and B. Sakmann. "Spatial profile of dendritic calcium transients evoked by action potentials in rat neocortical pyramidal neurones." In: *J Physiol.* 487 (1995), pp. 583–600.

[13] J. Waters and F. Helmchen. "Background Synaptic Activity Is Sparse in Neocortex". In: *J. Neurosci.* 26.32 (2006), pp. 8267–8277.